Water Vapor Concentration Enhancement in Compressed Humid Air Measured by Fourier Transform Infrared Spectroscopy

Gerald Koglbauer and Martin Wendland*

Institut für Verfahrens- und Energietechnik, Universität für Bodenkultur Wien, Muthgasse 107, 1190 Vienna, Austria

The knowledge of the dew point of compressed humid gases is needed for many new technical applications as, for example, the compressed air energy storage or the humid air turbine. The dew point concentration of water in compressed gases deviates with increasing pressure from the well-known ideal gas model. This deviation can be described either by the vapor pressure or the vapor concentration enhancement factor. There are only very few experimental data in a limited range available for the first factor and none at all for the latter. Here, a new method was developed and a new apparatus has been constructed to measure the vapor concentration enhancement factor by Fourier transform infrared spectroscopy. The apparatus is limited to a temperature range from (10 to 150) °C and pressures up to 25 MPa. The combined standard uncertainties (confidence level 68 %) of the new experimental data are 0.02 K for the temperature, 3.2 kPa for the pressure, and (0.13 to 1.15) % for the vapor concentration enhancement factor.

Introduction

Thermophysical properties of compressed humid air are needed for modern technologies as, for example, compressed air energy storage (CAES) or humid air turbine and are announced to be an IAPWS Certified Research Need (ICRN-14).[1] Properties of compressed humid air deviate with increasing pressure strongly from the well-known properties at ideal gas conditions. One important property is the dew point of compressed humid air. This is usually described by the vapor pressure enhancement factor f_W

$$f_W(T, p) = \frac{p_W}{p_W^0} \tag{1}$$

which is the ratio of the partial pressure of water $p_W = x_W\, p$ in saturated compressed humid air to the vapor pressure of pure water p_W^0. The enhancement factor f_W can be gained experimentally by measuring the mole fraction x_W as a function of the total pressure p and the temperature T. The mole fraction is usually determined by expanding the saturated compressed air and by measuring the water content and the dry air content gravimetrically or volumetrically. One difficulty of these measurements is that the amount of water per volume increases only slowly with increasing pressure while the amount of dry air per volume increases drastically, which results in a strongly decreasing mole fraction of water. Finally, a strongly decreasing mole fraction and slightly less strongly increasing pressure yields to a slow increase in the partial pressure p_W or the vapor pressure enhancement factor f_W. Thus, only a limited number of experimental data sets on f_W at (−35 to 75) °C and pressures up to 20 MPa with a few data points per isotherm are available up to now.[2−6]

A second way to describe the water enhancement in compressed air is given via the vapor concentration enhancement factor g_W

$$g_W(T, p) = \frac{c_W}{c_W^0} \tag{2}$$

which is the ratio of the water concentration c_W (in moles or mass per unit volume) in saturated compressed humid air to the saturated vapor density c_W^0 of pure water. The relationship between f_W and g_W is given by the ratio of the compressibility factors, where Z and Z_W^0 are the compressibility factors of the saturated humid gas and pure water vapor, respectively.

$$g_W = f_W \frac{Z_W^0}{Z} \tag{3}$$

The water concentration c_W increases, similar to the partial pressure, slowly with an increasing total pressure. Thus, a direct measurement of the water concentration c_W in compressed humid air at saturation, which is possible by spectrometry, is a straight forward and sensitive way to gain the water enhancement effect now described by the factor g_W. Here, Fourier transform infrared (FTIR) spectroscopy was chosen because the absorbance of IR light by water vapor is very sensitive and proportional to the per unit volume concentration.

For this new method, an apparatus was developed where a high-pressure view cell was placed in the sample compartment of an FTIR spectrometer. The view cell was filled with air and a small amount of liquid water so that IR light absorbance could be measured in situ in the gas phase, which was inside the view cell in equilibrium with the relatively thin liquid phase. This method allows rapid and quite accurate measurements of the vapor concentration enhancement factor by relating the IR light absorbance in compressed air to that in saturated pure vapor. An additional calibration in a homogeneous compressed air sample with known humidity content is needed to correct for the effect of the gas density on the FTIR spectra.

Measurements of the vapor concentration enhancement factor g_W in compressed humid air have been done at nine isotherms

* Corresponding author. Tel.: +43-1-3709726-212. Fax: +43-1-3709726-210. E-mail: martin.wendland@boku.ac.at.

10.1021/je700057x CCC: $37.00
Published on Web 08/01/2007

Table 1. Composition of the Synthetic Air and Its Uncertainties

component	mole fraction 100 x	relative uncertainty %
argon	0.9022	± 0.04
oxygen	20.954	± 0.01
nitrogen	balance	

between (20 and 140) °C and for pressures up to 25 MPa. The combined standard uncertainties (confidence level 68 %) of the g_W measurements are given with 1.15 % at 20 °C, 0.73 % at 30 °C, 0.49 % at 40 °C, 0.34 % at 50 °C, 0.24 % at 60 °C, 0.14 % at 80 °C, and 0.13 % at 100 °C and higher.

Experimental Section

Chemicals. Water of p.a. (pro analysi) grade was purchased by Merck company (Darmstadt, Germany) with a conductivity of less than 1 μS/cm at 25 °C. Synthetic carbon dioxide-free air was produced gravimetrically and analyzed in conformity with ISO 6143 by Linde company (Unterschleissheim, Germany) for a group of research institutes involved in the EC project advanced adiabatic-compressed air energy storage (AA-CAES). The composition of the air and its certified uncertainties are given in Table 1.

Method. The absorbance A of IR light by the water molecules is related to their concentration c_W in the gas phase via the Beer Lambert law

$$A = -\log T = \log\left(\frac{I_0}{I}\right) = \epsilon \cdot c \cdot d \tag{4}$$

where T is the transmission of the IR light, I_0 is the intensity of the light source measured as background spectrum, and I the intensity of light transmitted through the sample gas phase (sample spectrum). The absorbance A is proportional to the concentration c_W of water in the sample gas phase and the path length d of the sample gas phase passed by the IR laser light beam. The extinction coefficient ϵ depends on the light absorbing substance. Thus, the vapor concentration enhancement factor can be measured conveniently via the ratio of the absorbance A in the compressed gas phase to the absorbance A^0 in the pure vapor at the vapor pressure of water.

$$g_W = \frac{c_W}{c_W^0} = \frac{A}{A^0} \cdot \frac{\epsilon^0 \cdot d^0}{\epsilon \cdot d} \tag{5}$$

The path length (i.e., the internal length of the view cell) d or d^0 in the compressed gas phase or the pure vapor, respectively, depends slightly on the pressure and temperature. Also the extinction coefficient ϵ or ϵ^0 of the compressed gas phase or the pure vapor, respectively, depends on the temperature and the pressure of the humid gas, because the density of the dry air components has a pronounced influence on the IR light absorbance spectrum of the water molecules. This is partly due to the well-known peak broadening. But also an influence of complexation between water and the gas molecules can be observed in the spectra that increases with the gas density. We introduce a correction constant k_ϵ gaining the following simple relation

$$g_W = \frac{c_W}{c_W^0} = \frac{A}{A^0} \cdot k_\epsilon \tag{6}$$

The correction constant k_ϵ is determined at each isotherm as a function of the pressure by calibrations in a homogeneous gas with a known concentration of water. The method of calibration is described in detail below. Corrections with k_ϵ are mainly to smaller values of g_W and do not exceed −25 %.

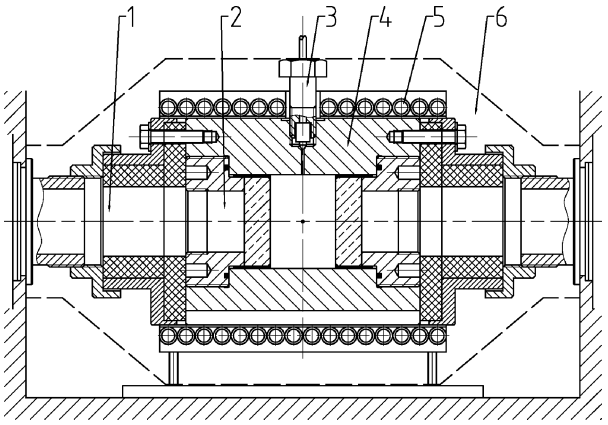

Figure 1. Design of the measuring cell and placement in the sample compartment of the FTIR spectrometer: 1, bellow; 2, sapphire window unit; 3, tube connector; 4, cell body; 5, thermostated jacket; 6, insulation.

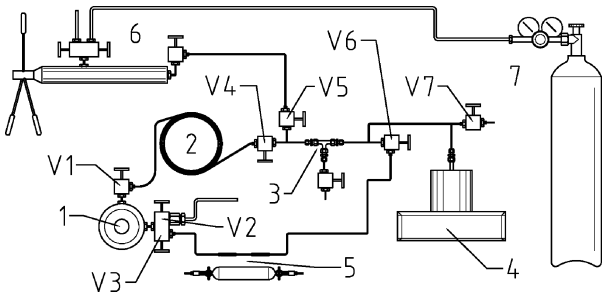

Figure 2. Scheme of the apparatus: 1, cell; 2, 1/16 in. capillary tube; 3, liquid trap; 4, digital piston gauge; 5, water port; 6, pressure generator; 7, gas bottle; V2, V7, vacuum port.

Apparatus and Procedure. Figure 1 shows the high-pressure view cell and its placement in the sample compartment of the FTIR spectrometer. The view cell has an internal volume of about 49 mL. It consists of a body machined from stainless steel (1.4571) and sapphire window units with poly(tetrafluoroethylene) sealings (Sitec, Swiss, model 742.0112). The sapphire windows absorb all light at wave numbers below 1800 cm^{-1} and thus disable the observation of the fingerprint spectra of water in this range. The optical length of the cell is 30 mm, and the optical diameter of the window units is 28 mm. It is thermostated with a jacket made from copper tubes that is insulated from the surrounding. The sapphire window units can be heated a little above the cell temperature by insulated heating pads to avoid condensation at the windows from the humid air inside the cell. The potassium bromide (KBr) windows of the spectrometer have been replaced by bellows to shelter the infrared light from the environment. They act simultaneously as positioning devices that keep the cell in a fixed position to avoid unnecessary scattering of the IR light because of the IR beam not being perpendicular to the sapphire windows.

Thus, the whole path of the IR laser light beam outside the cell (in the bellows and inside the spectrometer) can be flushed by nitrogen and dried by a mole sieve (4 Å molecular sieve for adsorption of water and carbon dioxide). Thus, the background spectrum measured with an evacuated view cell indicates a negligible presence of water (in the fingerprint range from (3975 to 3440) cm^{-1}) and carbon dioxide. The very sensitive absorbance band of carbon dioxide at 2370 cm^{-1} is a good indication of sufficient flushing and drying.

A scheme of the whole apparatus with the view cell (1), the gas delivery, the pressure measurement and the water port (5) is given in Figure 2. The gas delivery consists of a gas bottle (7) for the synthetic air and a pressure generator (6; Sitec, Swiss,

piston pump model 750.1060). Air is filled into the cell via a 1/16 in. capillary tube (2; stainless steel, 1.5 m length, 0.25 mm internal diameter, heated at 150 °C). Flow from the cell back to the gas delivery or pressure measurement is carefully avoided. Diffusion of the vapor through the capillary tube is negligible. The cell and the pressure measurement with a digital piston gauge (4) are separated by this capillary tube and a liquid trap (3) that is cooled to prevent water from entering the pressure gauge or the oil of the gauge from entering the view cell. However, liquid droplets have never been observed in the trap. In the water port, two different sample volumes can be included for calibration.

The following procedure was used for the measurement of the vapor concentration factor g_W. **(1)** A 5 mL sample of water was filled into the view cell at 5 °C with a syringe through the water port (5) while the valve V5 was closing off the pressure generator. The cell, while separated by V4 from the tubing system and the pressure measurement (V5 still closed), was then evacuated through V2 at 5 °C for at least 1 h to remove any dissolved gases, especially carbon dioxide. Meanwhile, the tubing system and the pressure gauge were evacuated through port V7 and prepared for the measurement. (2) The cell (filled with pure water) was then heated to the temperature of the desired isotherm. The sapphire window units were kept always 1 °C above the cell temperature during the temperature increase. The window temperature was lowered stepwise toward the cell temperature after reaching the desired isotherm and during equilibration. The progress of equilibration could be checked very sensitively by measuring FTIR spectra with medium resolution. No stirring was used to avoid water droplets or films at the windows. (3) The IR absorbance A^0 of saturated pure water vapor was measured after equilibrium was reached between the pure water vapor phase and the liquid water inside the cell. (4) Synthetic air was pressurized to about half the desired pressure inside the tubing system and the pressure gauge with valves V4 and V3 still closing off the cell. Then the valve V4 was opened so that the air can flow slowly into the cell through the capillary tube. The pressure then was increased slowly with the piston pump until the desired pressure was reached and valve V5 was closed. After equilibration, which again was checked by medium resolution spectra, the IR absorbance $A(T, p)$ of the water vapor in the compressed air was measured by high-resolution spectra. (5) The pressure was then raised along the isotherm and $A(T, p)$ is measured repeating step 4 for each measurement. The vapor concentration enhancement factor g_W can then be calculated by eq 6 for each measuring point from the ratio $A(T, p)/A^0$ if a calibration for k_ϵ is available. (6) For measurements at another isotherm, pressure was released from the cell, and it was flushed at 100 °C with nitrogen until dry.

Calibrations and Uncertainties. A thermostated bath (Gebr. Haake, Karlsruhe, Germany, type N6-B12) has been used to control the temperature of the measuring cell. The temperature was measured by a 25 Ω platinum resistance thermometer (Rosemount, USA, type 162 D) and indicated by a digital resistance bridge (F300, Automatic System Laboratory, UK). The thermometer has been calibrated prior to the measurements according to the International Temperature Scale of 1990 (ITS-90) at three fix points between (−40 and 156) °C by Landesamt für Mess- und Eichwesen Thüringen (Ilmenau, Germany, uncertainty within ± 2 mK). The combined standard uncertainty of the temperature measurement is estimated to be within 0.02 K. The pressure is measured by a digital piston gauge (Desgranges and Huot, Aubervilliers, France; model 21000 M, range, 0 to 30 MPa, uncertainty, ± (700 Pa + 10.0·10^{-5} p/Pa)). Thus, the maximum uncertainty of the pressure measurement is within 3.2 kPa.

Table 2. Method and Settings of the FTIR Spectrometer

parameter/method	setting
IR source	MIR globar (7500 to 370) cm^{-1}
aperture	3 mm
scanner velocity	20 kHz
scan time	30 scans
detector	RT-DLaTGS
sample gain	× 2
apodization	four point
resolution	1 cm^{-1}
acquisition mode	forward−backward
phase correction	power spectrum
phase resolution	1 cm^{-1}
zero-filling factor	32
integration method	peak bundle with baseline
integration range	(3975 to 3440) cm^{-1}
baseline nodes	(4135; 4000; 3400; 3050) cm^{-1}

The spectrometric method and the settings of the FTIR spectrometer (Tensor 27, Bruker Optik GmbH, Ettlingen) are given in Table 2. The absorbance A or A^0 is measured with a standard uncertainty of 0.035 absorbance units (u_A), which is mainly related to the stability of the mid-infrared (MIR) source and of the optical system. Drifts of the intensity of the MIR source are automatically compensated by the spectrometer software (Bruker OPUS 4.2) via offset correction. The measured absorbance increases with the temperature from $A = 10$ u_A at 20 °C to $A = 800$ u_A at 140 °C due to the increasing vapor density of water. This contributes to an uncertainty in g_W, which is strongly dependent on the temperature. At 100 °C and higher, the relative standard uncertainty $\Delta A/A^0$ thus would be below 0.02 %. This value will be taken as constant for all temperatures above 100 °C, because at these temperatures an additional uncertainty arises from a saturated absorption at some water peaks.

The correction constant k_ϵ in eq 6 can be determined for each isotherm as a function of pressure by calibration if the steps (1) to (5) of the g_W measurements are used, now with a known mass of water filled into the cell. This mass was chosen to be a little smaller than the mass that is solved at atmospheric pressure in saturated humid air. Thus, the content of the cell is a single, homogeneous gas phase with a water concentration c_W, which is constant with increasing pressure. Equation 6 now reduces to a simple relation for the correction factor

$$k_\epsilon = \frac{c_W}{c_W^0}\frac{A^0}{A} = \frac{A^0}{A} \tag{7}$$

The mass of water can be filled into the cell through the water port (5) as liquid for isotherms at 50 °C and higher or as gas for isotherms up to 70 °C. In the first case, liquid water was filled into a sample volume made from a 1/16 in. PEEK capillary tube (0.508 mm internal diameter) and was flushed with nitrogen at 1 MPa into the cell, which is thermostated at 2 °C. Then the water was frozen out in the cell at −10 °C for 1 h, and the cell was evacuated for another hour. In the second case, 10 mL of liquid water is filled with nitrogen at 0.1 MPa into a 200 mL glass cylinder. A gas−liquid equilibrium at a temperature above the desired isotherm was set inside the glass cylinder. The temperature was chosen so that the concentration in the gas phase at equilibrium was sufficient to achieve the desired water concentration in the cell after expansion of the gas phase from the glass cylinder to the evacuated cell while valve V1 was closed. The water concentration in the cell could now be checked

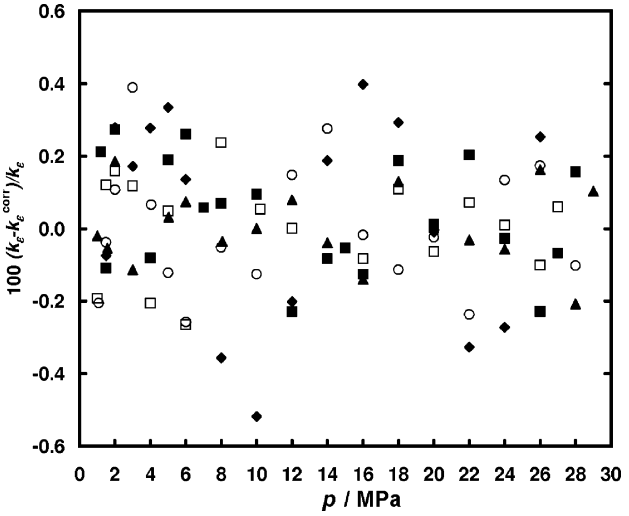

Figure 3. Deviations of the experimental values of k_ϵ (98 %, of saturation) from their correlation functions k_ϵ^{corr} at various isotherms: ◆, 20 °C; □, 50 °C; ▲, 80 °C; ○, 100 °C; ■, 120 °C.

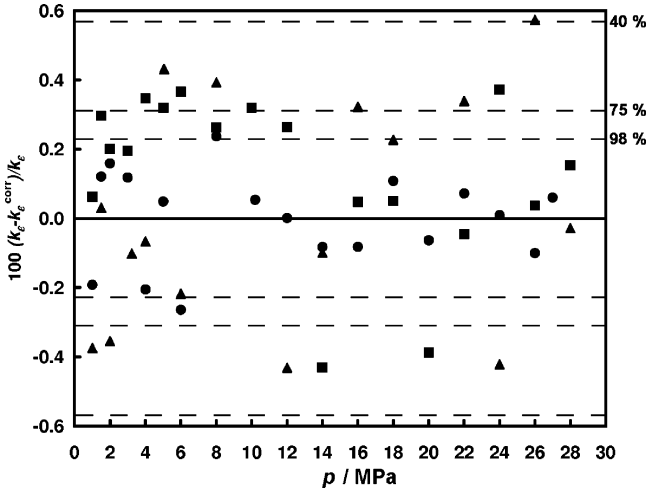

Figure 4. Deviations of the experimental values of k_ϵ at ●, 98 %, ■, 75 %;, and ▲, 40 % of saturation from the correlation function k_ϵ^{corr} at 50 °C. (The dashed lines give the estimated standard uncertainties of k_ϵ with eq 10 at 98 %, 75 %, and 40 % of saturation.)

by taking a spectrum, and it was adjusted if necessary. Again, the cell was cooled to −10 °C and evacuated. Then, steps (2) to (5) were used in a similar fashion as for the main measurements. Equilibration time for each calibration point was now much smaller with about 15 min because no liquid water is present in the cell.

Concerning the uncertainties, g_W is a function of temperature and pressure and is determined with eq 6 via measurements of the absorbance A and A^0 and a calibration with k_ϵ. Additionally, the uncertainties of the pressure and temperature measurement must be included for the measurement of A and the uncertainty of the temperature measurement for A^0. Thus, the combined standard uncertainty in g_W can be written by error propagation law as

$$\left(\frac{\Delta g_W}{g_W}\right)^2 = \left(\frac{\Delta p}{p}\right)^2 + 2\left(\frac{\Delta T}{T}\right)^2 + \left(\frac{\Delta A}{A^0}\right)^2 + \left(\frac{\Delta A}{A}\right)^2 + \left(\frac{\Delta k_\epsilon}{k_\epsilon}\right)^2 \quad (8)$$

With $|A^0| \le |A| \le |1.8\ A^0|$ this can be simplified to

$$\left(\frac{\Delta g_W}{g_W}\right)^2 = \left(\frac{\Delta p}{p}\right)^2 + 2\left(\frac{\Delta T}{T}\right)^2 + 2\left(\frac{\Delta A}{A^0}\right)^2 + \left(\frac{\Delta k_\epsilon}{k_\epsilon}\right)^2 \quad (9)$$

The combined standard uncertainty of the calibration has the same contributions from the measurements of A and A^0 and additional contributions from uncertainties in the water concentration c_W and from the correlation function (fifth-order polynomial), which is finally used in eq 6:

$$\left(\frac{\Delta k_\epsilon}{k_\epsilon}\right)^2 = \left(\frac{\Delta p}{p}\right)^2 + 2\left(\frac{\Delta T}{T}\right)^2 + 2\left(\frac{\Delta A}{A^0}\right)^2 + \left(\frac{\Delta k_\epsilon^{cW}}{k_\epsilon}\right)^2 + \left(\frac{\Delta k_\epsilon^{corr}}{k_\epsilon}\right)^2 \quad (10)$$

Figure 3 gives deviations of k_ϵ values at different temperatures from their respective correlation function. The deviations decrease with increasing temperature as it is expected from the $\Delta A/A^0$ contribution. They do not decrease below ± 0.2 % at 120 °C and higher temperatures, which can be accounted for by the water concentration and correlation contributions. The latter contribution was estimated to $\Delta k_\epsilon^{corr}/k_\epsilon = 0.10$ % (standard deviation).

Uncertainties of k_ϵ from the water concentration can result either from the fact that the water content during calibration corresponds to a g_W of about 0.98 or from diffusion through the capillary tube that is negligible at saturation but might lead to a slow decrease in the concentration during calibration.

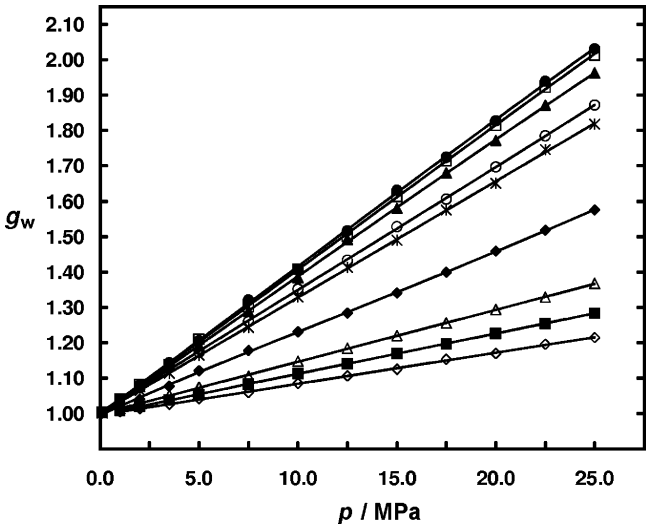

Figure 5. Vapor concentration enhancement factor g_W of compressed humid air, consistency of the experimental data (points) along isotherms: ●, 20 °C; □, 30 °C; ▲, 40 °C; ○, 50 °C; ∗, 60 °C; ◆, 80 °C; △, 100 °C; ■, 120 °C; ◇, 140 °C.

Measurements at 75 % and 40 % of saturation were done to estimate the uncertainty Δk_ϵ^{cW}. Figure 4 shows deviations of the measured k_ϵ values at 98 %, 75 %, and 40 % of saturation from the correlation function at the 50 °C isotherm. These measurements show no systematic deviations. The deviations of all three data sets are each within the uncertainties given by the first three contributions in eq 10. (These uncertainties, or standard deviations, are shown in Figure 4 as horizontal dashed lines.) Thus, there is no additional, systematic error from the subsaturation on k_ϵ. For the contribution Δk_ϵ^{cW}, only a loss of water in the cell because of diffusion in the capillary tube has to be taken into account. This systematic error was estimated by calculations of the unsteady diffusion in the capillary tube using a diffusion coefficient of water in air of $D_{W,A} = 3.1 \cdot 10^{-5}$ m²/s at 150 °C and 0.1 MPa[7] to $\Delta k_\epsilon^{cW}/k_\epsilon = \Delta k_\epsilon^{diff}/k_\epsilon = 0.10$ %. The diffusion coefficient decreases rapidly with the gas density, as can be shown by kinetic theory and a corresponding state model.[8] With a diffusion coefficient of $D_{W,A} = 7.1 \cdot 10^{-6}$ m²/s at 150 °C and

Table 3. Experimental Data for the Vapor Concentration Enhancement Factor g_W of Compressed Humid Air

	g_W								
p/MPa	t = 20 °C	t = 30 °C	t = 40 °C	t = 50 °C	t = 60 °C	t = 80 °C	t = 100 °C	t = 120 °C	t = 140 °C
0.1	1.0037	1.0035	1.0030	1.0039	1.0020	1.0013			
1.0	1.0409	1.0406	1.0342	1.0355	1.0341	1.0210	1.0141	1.0082	1.0050
2.0	1.0799	1.0822	1.0759	1.0733	1.0648	1.0408	1.0272	1.0200	1.0139
3.5	1.1433	1.1387	1.1362	1.1299	1.1140	1.0769	1.0519	1.0383	1.0263
5.0	1.2048	1.2102	1.1912	1.1724	1.1642	1.1204	1.0740	1.0535	1.0425
7.5	1.3208	1.3018	1.2886	1.2594	1.2435	1.1777	1.1051	1.0829	1.0594
10.0	1.4090	1.4083	1.3844	1.3515	1.3288	1.2312	1.1475	1.1126	1.0849
12.5	1.5167	1.5016	1.4921	1.4330	1.4125	1.2838	1.1837	1.1408	1.1061
15.0	1.6314	1.6134	1.5798	1.5279	1.4897	1.3405	1.2200	1.1694	1.1248
17.5	1.7241	1.7139	1.6796	1.6056	1.5751	1.3991	1.2555	1.1965	1.1532
20.0	1.8270	1.8143	1.7715	1.6968	1.6509	1.4590	1.2931	1.2259	1.1695
22.5	1.9389	1.9226	1.8714	1.7849	1.7460	1.5178	1.3283	1.2547	1.1954
25.0	2.0310	2.0134	1.9627	1.8721	1.8178	1.5752	1.3673	1.2835	1.2143

Table 4. Combined Standard Uncertainties (Confidence Level 68 %) of the Experimental Data for the Vapor Concentration Enhancement Factor g_W of Compressed Humid Air

	t = 20 °C	t = 30 °C	t = 40 °C	t = 50 °C	t = 60 °C	t = 80 °C	t = 100 °C	t = 120 °C	t = 140 °C
$\Delta p/p$	0.00010	0.00010	0.00010	0.00010	0.00010	0.00010	0.00010	0.00010	0.00010
$\Delta T/T$	0.00007	0.00007	0.00006	0.00006	0.00006	0.00006	0.00005	0.00005	0.00005
$\Delta A/A^0$	0.00565	0.00360	0.00236	0.00162	0.00103	0.00037	0.00020	0.00020	0.00020
$\Delta k_\epsilon^{diff}/k_\epsilon$	0.00050	0.00050	0.00050	0.00050	0.00050	0.00050	0.00050	0.00050	0.00050
$\Delta k_\epsilon^{corr}/k_\epsilon$	0.00100	0.00100	0.00100	0.00100	0.00100	0.00100	0.00100	0.00100	0.00100
$\Delta k_\epsilon/k_\epsilon$	0.0081	0.0052	0.0035	0.0026	0.0018	0.0013	0.0012	0.0012	0.0012
$\Delta g_W/g_W$	0.0115	0.0073	0.0049	0.0034	0.0024	0.0014	0.0013	0.0013	0.0013

1 MPa, the uncertainty is smaller with $\Delta k_\epsilon^{cw}/k_\epsilon = \Delta k_\epsilon^{diff}/k_\epsilon =$ 0.05 %.

Finally, the combined standard uncertainty of the measurements is given by

$$\frac{\Delta g_W}{g_W} = \sqrt{2\left(\frac{\Delta p}{p}\right)^2 + 4\left(\frac{\Delta T}{T}\right)^2 + 4\left(\frac{\Delta A}{A^0}\right)^2 + \left(\frac{\Delta k_\epsilon^{diff}}{k_\epsilon}\right)^2 + \left(\frac{\Delta k_\epsilon^{corr}}{k_\epsilon}\right)^2} \quad (11)$$

The combined standard uncertainty has contributions from four temperature and two pressure measurements (for both the main measurement and the calibration) and from four measurements of the absorbance (A and A^0 for both the main measurement and the calibration). There are two additional contributions from the calibration: a contribution from the diffusion in the capillary tube during the calibration, which can lead to a systematic error in the concentration, and a contribution from the correlation of k_ϵ. The uncertainty in the absorbance is the dominating contribution. It yields to a relatively large uncertainty at low temperatures where A^0 has small values and a very low uncertainty at the highest temperature. The combined standard uncertainty (confidence level 68 %) in g_W ranges from 1.15 % at 20 °C to 0.13 % at 100 °C and higher (Table 4).

The uncertainties at lower temperatures could be improved by larger absorbance values or higher stability of the optical system of the spectrometer. A larger absorbance can be achieved by using different window material or a longer path length d. To get a sufficient absorbance at, for example, 20 °C, the path length of the cell has to be approximately five times longer. But, this could lead to other and perhaps unexpected disturbances.

Results and Discussion

Measurements of the vapor concentration enhancement factor g_W were done at isotherms between (20 and 140) °C with at least 12 pressure values per isotherm up to 25 MPa. Results of the measurements are shown in Table 3. Uncertainties of these data estimated with eq 11 are given for each isotherm in Table 4. The experimental g_W data is displayed in Figures 5 and 6 over the pressure or temperature, respectively. As a demonstration of the consistency of the data, simple polynomial correlation functions of the single isotherms or isobars are also given in the diagrams. Deviations of the experimental data to the isothermal correlations in Figure 5 are within ± 1 %, which is within the experimental uncertainty. Thus, the consistency of the experimental data confirms the combined standard uncertainties of eq 11 and Table 4. The deviations to the isobaric correlations in Figure 6 are somewhat larger with ± 3 %. This is partly due to the more complicated temperature dependence of the data that does not fit completely to the fourth-order correlation function.

No experimental values for the vapor concentration enhancement factor g_W was found in the literature. Only experimental data for the vapor pressure enhancement factor f_W in a limited temperature range from (−35 to 75) °C and pressures up to 20

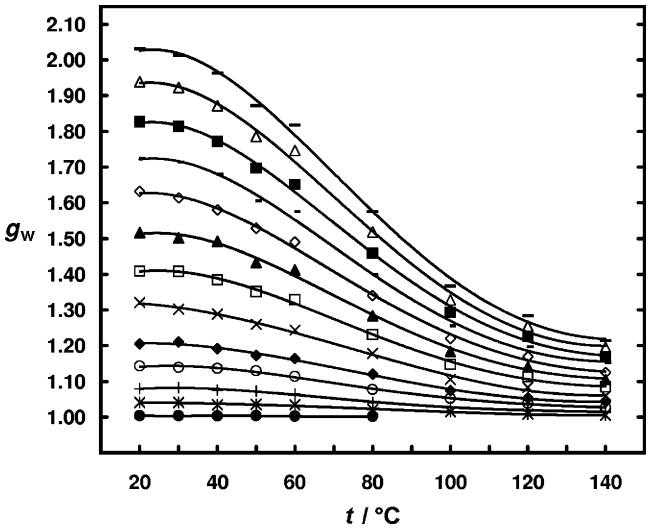

Figure 6. Vapor concentration enhancement factor g_W of compressed humid air, consistency of the experimental data (points) along isobars: ●, 0.1 MPa; ∗, 1.0 MPa; +, 2.0 MPa; ○, 3.5 MPa; ♦, 5.0 MPa; ×, 7.5 MPa; □, 10.0 MPa; ▲, 12.5 MPa; ◇, 15.0 MPa; −, 17.5 MPa; ■, 20.0 MPa; △, 22.5 MPa; —, 25.0 MPa.

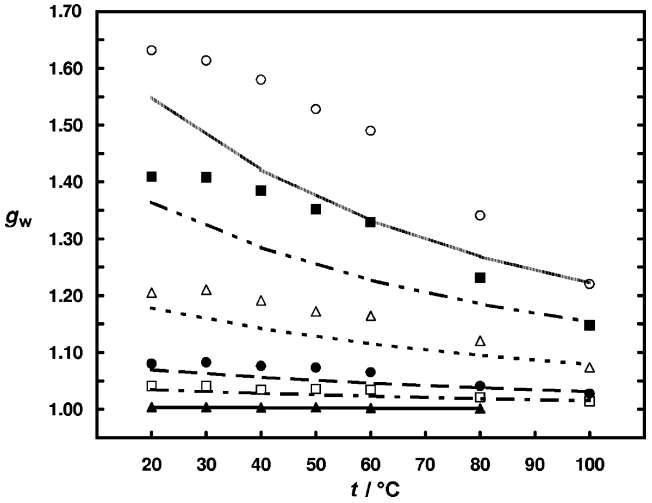

Figure 7. Vapor concentration enhancement factor g_W of compressed humid air. Comparison of the present experimental data (symbols) with data from a model of Wylie and Fisher[5] (lines). ▲/—, 0.1 MPa; □/– -, 1 MPa; ●/– –, 2 MPa; △/- - -, 5 MPa; ■/– - -, 10 MPa; •••, 15 MPa.

MPa are available.[2−5] Wylie and Fisher[5] give values for g_W at (0 to 100) °C and (0.1 to 15) MPa calculated with a virial equation model, which is based on their own experimental f_W data for (20, 50, and 75) °C. The present experimental data for g_W is compared to these data of Wylie and Fisher in Figure 7. Both data sets agree well at 100 °C but deviate with lower temperatures with a maximum of 20 % at 50 °C and again better agreement at 20 °C. The agreement at 100 °C is rather surprising because no experimental data above 75 °C was available for the model at that time.

We expect that the discrepancies of the model of Wylie and Fischer to the experimental values for g_W are based on the fact that for the model only long range interactions and no complexation between water and the gas molecules are taken into account. This yields to a wrong extrapolation of the model from the very limited temperature range to higher temperatures or from one kind of property, for example, f_W, to an other type of property, for example, g_W. There is experimental and theoretical evidence for van der Waals complexes of water and nitrogen or oxygen in the atmosphere that is of importance for the understanding of the atmospheric absorbance of solar light, that is, the greenhouse effect. Kjaergaard et al.[9] give a good overview of the available literature on these complexes. They have also calculated the conformations of water−nitrogen and water−oxygen complexes and their infrared activities by ab initio methods. Experimental observations of water−nitrogen complexes[10] and water−oxygen complexes[11] by high-resolution IR matrix isolation spectroscopy are also available.

All of these studies show a small shift in the vibrational frequencies and intensities of the bound water molecules that has an effect on the water vibration FTIR spectra in our measurements. Both free and bound water are included in the integration of the spectra to the absorbance A and thus also in g_W and k_ϵ. For a rough approximation of the fraction of water that is bound in complexes, we use the ab initio data of Svishchev et al.[12] who give values for dimerization enthalpies and entropies at 298.16 K and 1 atm for water−oxygen and water−nitrogen dimers. At the given conditions, the mole fraction of the water−nitrogen dimer in saturated humid air is approximately $16 \cdot 10^{-6}$. This corresponds to 0.05 % of the total water content at saturation. By raising the pressure to 20 MPa, the fraction of water bound in water−nitrogen complexes increases to 10 % of the total water content. The amount bound in water−oxygen dimeres is about half of that in the water−nitrogen dimeres. Also, larger complexes are expected at higher gas densities. We have further studied the influence of complexation on the water enhancement by measurements in pure nitrogen, argon, and carbon dioxide, which will be discussed in a subsequent paper.[13]

Conclusions

A new method for the measurement of the vapor concentration enhancement factor was developed and verified with a new apparatus. It offers a much easier and faster possibility to measure the vapor enhancement in compressed gases than previous methods. With the new data for compressed humid air, a much broader and better data base for the development of models for the thermophysical properties of compressed humid air is now available. There is an evidence for complexation of water and nitrogen or oxygen that should be considered for the improvement of models.

Literature Cited

(1) International Association for the Properties of Water and Steam. IAPWS Certified Research Need-ICRN. Thermophysical Properties of Humid Air and Combustion-Gas Mixtures. ICRN-14, 2002.
(2) Pollitzer, F.; Strebel, E. Über den Einfluss indifferenter Gase auf die Sattdampfkonzentration von Flüssigkeiten. Z. *Phys. Chem.* **1924**, *110*, 768−785.
(3) Webster, T. J. The Effect on Water Vapor Pressure of Superimposed Air Pressure. *J. Soc. Chem. Ind., London* **1950**, *69*, 343−346.
(4) Hyland, R. W.; Wexler, A. The Enhancement of Water Vapor in Carbon Dioxide-Free Air at 30, 40, and 50°C. *J. Res. Natl. Bur. Stand. A* **1973**, *77*, 115−131.
(5) Hyland, R. W. Correlation of the Second Interaction Virial Coefficients and Enhancement Factors for Moist Air. *J. Res. Natl. Bur. Stand. A* **1975**, *79*, 551−560.
(6) Wylie, R. G.; Fisher, R. S. Molecular Interaction of Water Vapor and Air. *J. Chem. Eng. Data* **1996**, *41*, 133−142.
(7) Massman, W. J. A Review of Molecular Diffusivities of H_2O, CO_2, CH_4, CO, O_3, SO_2, NH_3, N_2O, NO, and NO_2 in Air, O_2 and N_2 near STP. *Atmos. Environ.* **1998**, *32*, 1111−1127.
(8) Slattery, J. C.; Bird, R. B. Calculation of the Diffusion Coefficient of Dilute Gases and of the Diffusion Coefficient of Dense Gases. *AIChE J.* **1958**, *4*, 137−142.
(9) Kjaergaard, H. G.; Low, G. R.; Robinson, T. W.; Howard, D. L. Calculated OH-Stretching Vibrational Transitions in the Water-Nitrogen and Water-Oxygen Complexes. *J. Phys. Chem.* **2002**, *106*, 8955−8962.
(10) Coussan, S.; Loutellier, A.; Perchard, J. P.; Racine, S.; Bouteiller, Y. Matrix Isolation Infrared Spectroskopy and DFT Calculations of Complexes between Water and Nitrogen. *J. Mol. Struct.* **1998**, *471*, 37−47.
(11) Cooper, P. D.; Kjaergaard, H. G.; Langford, V. S.; McKinley, A. J.; Quickenden, T. I.; Robinson, T. W.; Schofield, D. P. Infrared Identification of Matrix Isolated $H_2O \cdot O_2$. *J. Phys. Chem. A* **2005**, *109*, 4274−4279.
(12) Svishchev, I. M.; Boyd, R. J. van der Waals Complexes of Water and Nitrogen: Infrared Spectra and Atmospheric Implications. *J. Phys. Chem. A* **1998**, *102*, 7294−7296.
(13) Koglbauer, G.; Wendland, M. Water Vapor Concentration Enhancement in Compressed Humid Nitrogen, Argon, and Carbon Dioxide Measured by Fourier Transform Infrared Spectroscopy. *J. Chem. Eng. Data* **2007**, submitted for publication..

Received for review February 1, 2007. Accepted June 21, 2007. A part of the present research was financed within the European Community FP5 project "Advanced Adiabatic Compressed Air Energy Storage" (AA-CAES).

JE700057X